Technical Report Documentation Page

1. Report No. R-1517	**2. Government Accession No.**	**3. MDOT Project Manager**
4. Title and Subtitle Analysis of Stress Distribution in Link Plates Used for Suspending Bridge Beams		**5. Report Date** September 2008
		6. Performing Organization Code
7. Author(s) Peter O. Jansson, P.E.		**8. Performing Org. Report No.**
9. Performing Organization Name and Address Michigan Department of Transportation Construction and Technology Division P.O. Box 30049 Lansing, MI 48909		**10. Work Unit No. (TRAIS)**
		11. Contract No.
		11(a). Authorization No.
12. Sponsoring Agency Name and Address Michigan Department of Transportation Construction and Technology Division P.O. Box 30049 Lansing, MI 48909		**13. Type of Report & Period Covered** Final Report
		14. Sponsoring Agency Code 07 TI-2097
15. Supplementary Notes		

16. Abstract

This report investigates the stress distribution in link plates with varying amounts of material behind the link plate pins. The link plates of I-94 EB over Norfolk Southern Railroad and Portage Creek, Bridge ID R02-39022, were not fabricated in accordance with AASHTO bridge design code due to less than the required amount of material behind the pin. These link plates were modeled, along with a similarly sized link plate with the required amount of material behind the pin, using finite element analysis verified by full scale tensile testing. End-of-plate stresses were found to increase dramatically as material behind the pin was removed; stresses immediately adjacent to the pin increased significantly, the overall yield and ultimate capacity decreased, and the mid-plate stresses remained relatively unchanged. The link plates of R02-39022 were removed and replaced with correctly sized link plates; one of the salvaged plates was tested and found to have yielded and entered the strain hardening region. A method of estimating effective stresses in link plates with less than the required amount of material behind the pin was developed.

17. Key Words Link plate, pin and hangers, steel bridges, finite element analysis		**18. Distribution Statement** No restrictions. This document is available to the public through the Michigan Department of Transportation.	
19. Security Classification - report Unclassified	**20. Security Classification -page** Unclassified	**21. No. of Pages** 40	**22. Price**

MICHIGAN DEPARTMENT OF TRANSPORTATION
MDOT

Analysis of Stress Distribution in Link Plates Used for Suspending Bridge Beams

Peter O. Jansson, P.E.

Structural Research Unit
Construction and Technology Division
Research Project TI-2097
Research Report No. R-1517

Lansing, Michigan
September 2008

Acknowledgements

The author would like to thank the following Department staff for their contributions to the project: Dave Juntunen and Rebecca Curtis for initiating the project, Roger Till and Steve Kahl for project guidance, Chris Davis, Rich Ginther, and Jon Todd for assistance with fabrication and testing the specimens and Greg Palmer for assistance with instrumentation and data acquisition.

Table of Contents

1. Introduction

Michigan has a large inventory of bridges with link plate assemblies, also known as pin and hanger assemblies; approximately 35 percent of the 2914 bridges with steel beams owned by the Michigan Department of Transportation (MDOT) currently have this detail. The link plate detail was developed to relocate joints away from bridge piers to reduce the damage to piers and beam ends caused by leaking joints. All available information indicates that by 1983[1] MDOT had discontinued the use of the pin and hanger detail on new structures due to several performance concerns including corroded and cracked link plates and beam ends in contact, but many in-service bridges still have them.

One structure with the pin and hanger detail, I-94 EB over Norfolk Southern Railroad and Portage Creek, MDOT Bridge ID R02-39022, was found to have non-standard fabricated link plates. R02-39022 is a four span bridge with six beam lines constructed in 1964. The beams are cantilevered over both the first and third piers, and linked to the beams of the second and third spans by pin and hanger assemblies. The beams are simply supported at the middle pier. Figure 1 shows the general elevation plan of R02-39022, with the link plate locations circled on the superstructure.

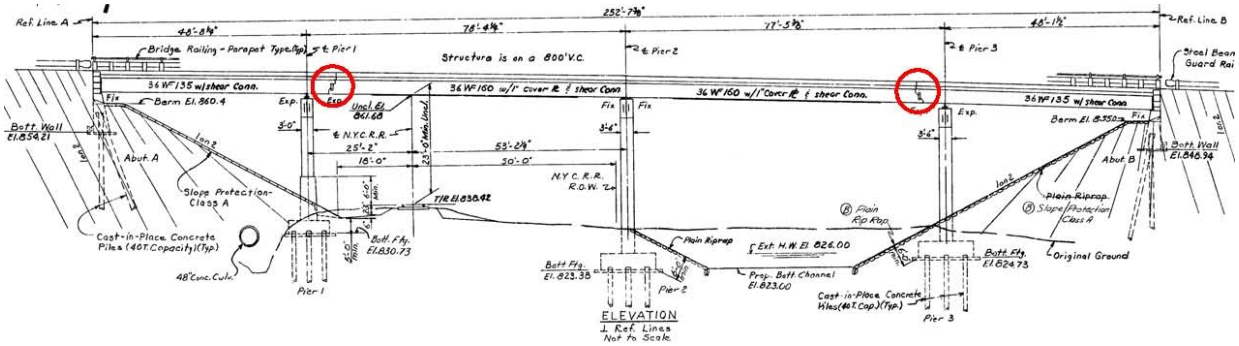

Figure 1
R02-39022 general elevation plan of structure, link plate locations circled

Current American Association of State Highway and Transportation Officials (AASHTO) Bridge Design Specifications[2,3] require the net section across the pin-hole of a link plate to be not less than 140 percent of the required net section, and the net section in back of the pin-hole to be not less than 100 percent of the required net section of the body of the link plate. This accounts for stress concentrations that develop around the pin-hole.

For the subject structure in this investigation, R02-39022, the link plate required net section per the AASHTO Bridge Design Specifications is 2.1 in^2, requiring the net section across the pin-holes to be no less than 2.94 in^2, and the area behind the pin to be no less than 2.1 in^2. With a thickness of 0.875 inch, the length of material as measured from the back of the pin-hole should have been no less than 2.1/0.875, or 2.4 inches. However, as seen in Figure 2, the fabrication plans only indicated a length of material behind the pin of one inch. These plates were removed

[1] Personal communications with MDOT Design and Construction and Technology staff, 2008.
[2] Standard Specifications for Highway Bridges, Sixteenth Edition, AASHTO, 2002.
[3] LRFD Bridge Design Specifications, Fourth Edition, AASHTO, 2007.

and replaced in 2007 with new plates. Several plates were salvaged from R02-39022; for the two salvaged link plates with material behind the pin still attached, the length of material behind the pin was measured and found to be 0.92 inch and 0.70 inch due to section loss, with additional section loss across the thickness of the link plate. The link plate with 0.70 inch behind the pin is shown in Figure 3.

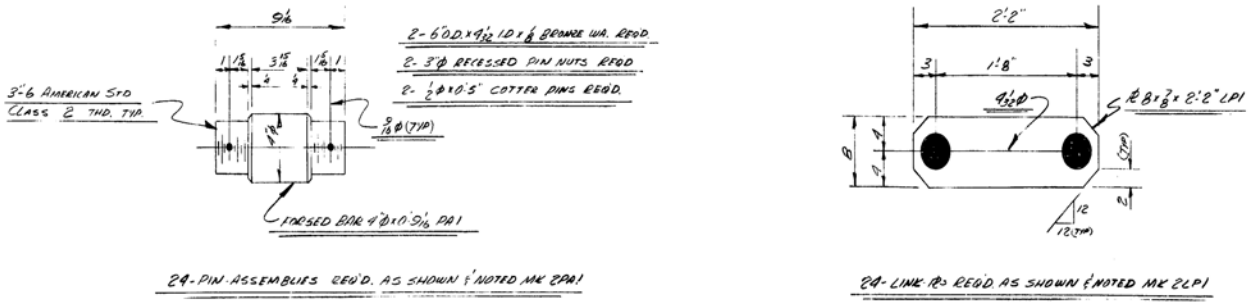

Figure 2
R02-39022 pin and hanger as-built fabrication plans

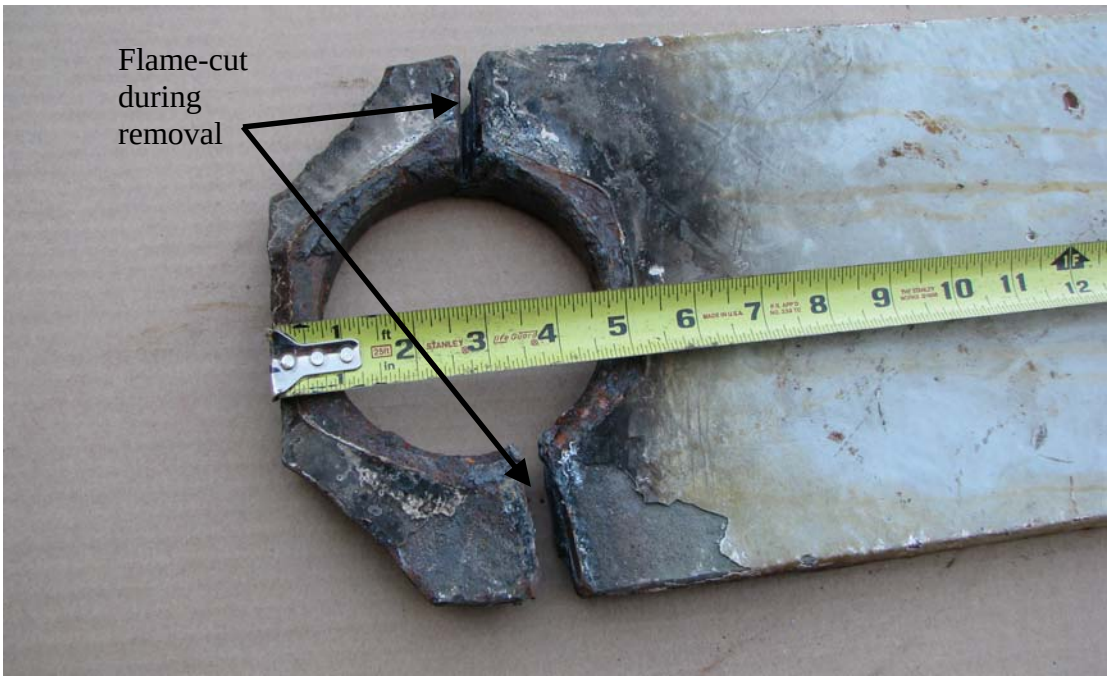

Figure 3
Salvaged link plate from R02-39022 with 38 percent section loss behind pin-hole

To study the stress distribution in link plates when the area behind the pin is less than required by AASHTO Bridge Design Specifications, two finite element models (FEM) were created; the link plate as fabricated for R02-39022 with only one inch of material behind the pin-hole was compared to a second link plate designed in accordance with AASHTO specifications with three inches of material behind the pin-hole. Full sized test specimens were fabricated and tensile tested to validate the finite element analysis (FEA). Additional FEM's were created to further investigate the stress in link plates with varying amounts of material behind the pin-hole and to develop methods for estimating stress in non-standard link plates.

2. Background

It is believed that the AASHTO net section requirements for link plates originated in part from the American Railway Engineering Association (AREA), whose 1911 Manual[4] specified that pin-connected riveted tension members shall have a net section through the pin-hole of 125 percent, and a net section behind the pin-hole of 100 percent, of the net section of the body of the member. This specification was later revised[5] to require that the net section across the pin-hole requirement be a minimum of 140 percent, the current AASHTO specification.

Johnston[6] developed empirical formulas to predict the general yield and ultimate strength of link plates based on testing of various sized plates. Three ultimate failure modes were identified: (1) Tension failure in the net section at one side of the pin, (2) Crushing and shearing failure below the pin, in some cases followed by a tearing fracture in "hoop" tension after considerable deformation, and (3) "Dishing" failure of thin plates that are laterally unrestrained. For the tests conducted by Johnston that had link plate dimensions similar to the experimental link plates tested for this project, no dishing was evident.

Stress distribution in link plates was previously investigated by MDOT; Juntunen[7] investigated live load stresses in in-service link plates as well as laboratory tensile testing of a scaled link plate model to study stress concentrations and fatigue behavior. Three bridges with high Average Daily Truck Traffic (ADTT) were instrumented with strain gauges on the link plates: I-96 over M-52 South of Webberville, S02-33085; M-14/US-23 over the Huron River and Conrail Railroad, R01-81075; and I-75 over Toledo/Dix, S21-82191. The instrumentation and data collected for two link plates on S21-82191 is not covered here because data collected from strain gauges placed between the pins did not address the stress concentrations around the pin, and the one strain gauge placed close to the pin actually had lower stress values than those in the middle of the plate, which was attributed to corrosion and the link plates being frozen in place.

S02-33085 had new link plates installed in 1992 measuring 30 inches by 8.5 inches by 0.875 inches, with 4 inch diameter holes spaced 20 inches center to center. Two link plates were instrumented with strain gauges as seen in Figures 4a and 4b. For each link plate instrumented, gauge 1 was placed in the middle of the plate, gauge 2 was placed next to the pin, and gauge 3 was placed behind the pin. To gain a better understanding of the stress concentrations around the pin, gauges 2 and 3 for the link plate in Figure 4a were placed one inch from the pin and gauges 2 and 3 for the link plate in Figure 4b were placed directly adjacent to the pin.

[4] *Manual of the American Railway Engineering Association: Definitions, Specifications, and Principles of Practice,* American Railway Engineering Association, 1911 Edition.
[5] *Manual of the American Railway Engineering Association: Definitions, Specifications, and Principles of Practice,* American Railway Engineering Association, 1921 Edition.
[6] *Pin-connected Plate Links,* American Society of Civil Engineers, Johnston, Bruce G., 1939.
[7] MDOT Research Report R-1358, *Study of Michigan's Link Plate Assemblies*, 1998.

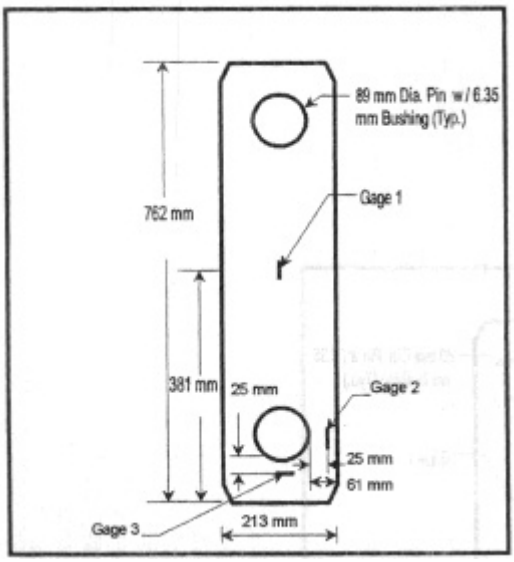

Figure 4a

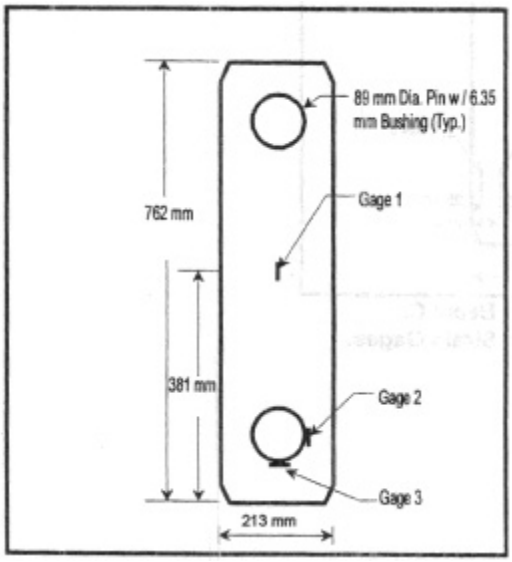

Figure 4b

Figures 4a and 4b
Instrumented link plates on S02-33085, dimensions are in SI units

Traffic was restricted over the link plates in Figures 4a and 4b while the strain gauges were installed, to facilitate accurate collection of live load stresses. The live load stresses were measured over a two hour period for each link plate, during which 218 trucks crossed the structure for the link plate in Figure 4a, and 246 trucks crossed the structure for the link plate in Figure 4b. The ratio of live load stresses from gauge 2 to gauge 1 was 2.7 for the link plate in Figure 4a, and 3.8 for the link plate in Figure 4b. The maximum live load stress occurrences at gauge 2 were 9.5 ksi and 8.5 ksi for the link plates in Figures 4a and 4b, respectively. The stress concentration factors for the instrumented link plates of S02-33085 were calculated based on Equation 1.

$$S_{r(netsection)} = S_{r(gauge2)} \times \frac{D_{(net/gross)}}{D_{(gauge2/gauge1)}} \qquad \text{(Eq.1)}$$

where:

$S_{r(\text{net section})}$ = estimated effective stress at the net section of the link plate, neglecting the stress concentration at the pin-hole (ksi)
$S_{r(\text{gauge 2})}$ = effective stress at gauge 2 (ksi)
$D_{(\text{net/gross})}$ = theoretical stress increase ratio from gross section at center of link plate to net section of the link plate (ksi)
$D_{(\text{gauge2/gauge1})}$ = stress increase ratio from gauge 1 to gauge 2 (ksi)

The stress concentration factor, which represents the ratio of the stress at the net section including the stress concentration at the pin to the stress at the net section neglecting the stress concentration at the pin, can be defined as $S_{r(\text{gauge 2})}$ divided by $S_{r(\text{net section})}$. These values for the link plates in Figures 4a and 4b were 1.27 and 2.02, respectively. The difference in the stress concentration factors is due to the placement of the strain gauges. Since strain gauge 2 is closer

to the pin in Figure 4b than it is in Figure 4a, higher stress is recorded relative to the stress at the net section neglecting the stress concentration at the pin.

R01-81075 is a non-redundant structure which received new link plates in 1990. One of the link plates was instrumented as seen in Figure 5, measures 54 inches by 15 inches by 1.5 inches, and has two 5.5-inch diameter pins spaced at 30 inches. Gauge 1 was placed in the middle of the link plate and gauge 2 was placed directly adjacent to the pin.

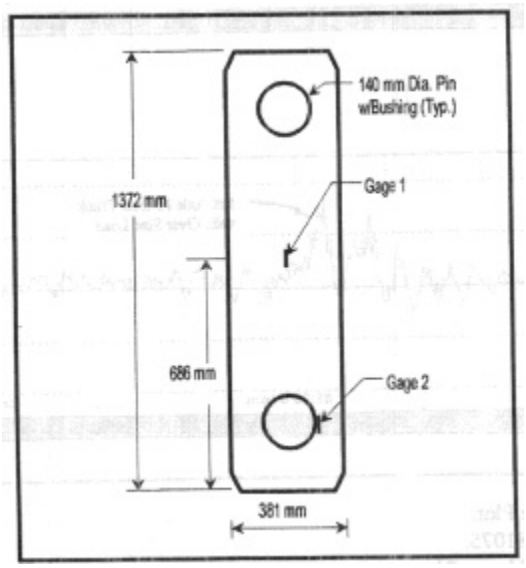

Figure 5
Instrumented link plate on R01-81075, dimensions in SI units

The strain gauges were installed similarly to the strain gauges for S02-33085, and data were collected for a time period of two hours, during which the maximum stress occurrence at gauge 2 was 18.5 ksi. The data from gauge 1 were not available, so gauge 2 could not be compared directly with gauge 1. However, the stress concentration factor was estimated to be 2.28 based on the geometry of the link plate, calculated using the following equation. [8]

$$k = 3.00 - 3.13\left(\frac{2r}{D}\right) + 3.66\left(\frac{2r}{D}\right)^2 - 1.53\left(\frac{2r}{D}\right)^3 \qquad \text{(Eq.2)}$$

where:

k = the stress concentration factor based on an axially loaded plate with infinite length in the direction of loading
r = radius of the hole in the plate
D = width of the plate

[8] *Roark's Formulas for Stress and Strain*, Sixth Edition, Young, Warren C., 1989.

Laboratory testing was conducted on a scaled model of a link plate, as seen in Figure 6. The dimensions were 14.25 inches by 4 inches by 0.4 inches, with two 1.61 inch diameter pins spaced at 9.5 inches center to center. Similar to the placement seen in Figures 4b and 5, strain gauges were placed in the middle of the plate (Gage A) and on the side of the pin immediately adjacent to the pin (Gage C), and also at the edge of mid-plate (Gage B)

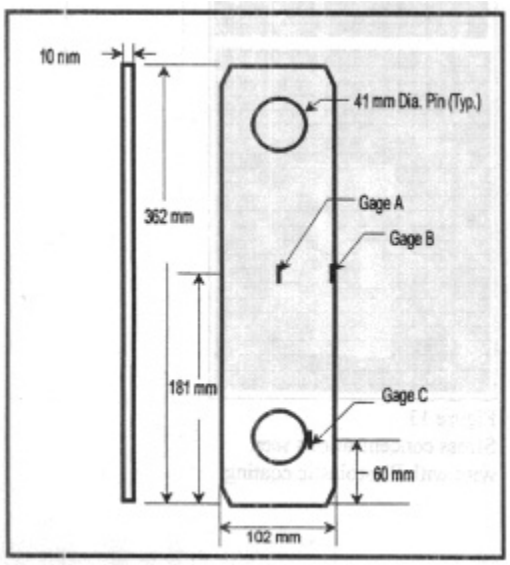

Figure 6
Scaled model link plate from laboratory testing, dimensions in SI units

The average stress concentration factor calculated from three tests was 2.3 and the stress at gauge C ranged from 3.5 to 4.1 times the stress at gauge A, and from 3.1 to 3.6 times the stress at gauge B. This was comparable to the results found with the link plate testing illustrated in Figure 4b. The stress concentration factor and ratios for the laboratory testing are greater than the link plate testing illustrated in Figure 4a because the strain gauge next to the pin in Figure 4a was offset one inch.

3. Linear Elastic Finite Element Analysis

GTStrudl V.29 software was used to conduct two-dimensional FEA on the R02-39022 link plate and the link plate with the AASHTO design. Both plates were eight inches wide and 0.875 inch thick; the plate with the AASHTO design had an additional two inches of material behind the pin. SBHQ6 plate elements were used to construct two models, as seen in Figures 7 and 8. The plates were fixed at one pin-hole and load was transferred to the plates at the other pin-hole via stiff compression-only members modeling the pin. For ease of modeling extra material was only added at one end of the longer plate and the corners were not coped; the models showed very low stress in the corners. Linear elastic material properties were used, limiting the analyses to pre-yield behavior. A load of 74.56 kips, representing the factored dead load plus live load on one link plate from a MI-18 truck[9], as seen in Figure 9, was applied to both link plates in the longitudinal (x) direction. In Figure 9, NL designates normal axle loading and DL denotes designated axle loading (DL was used for load application in the models).

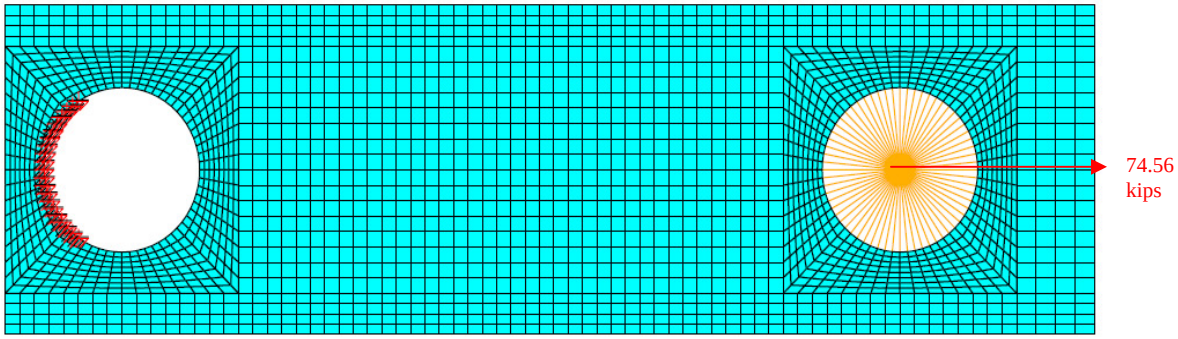

Figure 7
Link plate with three inches of material behind pin

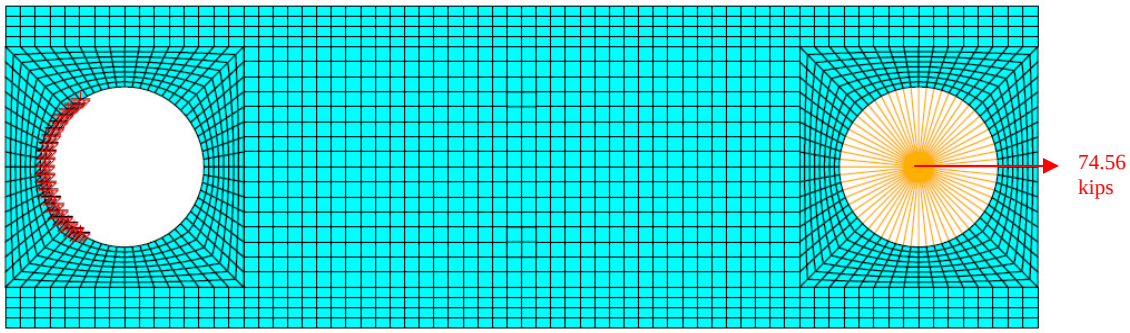

Figure 8
Link plate with one inch of material behind pin

[9] MDOT Bridge Analysis Guide, 2003.

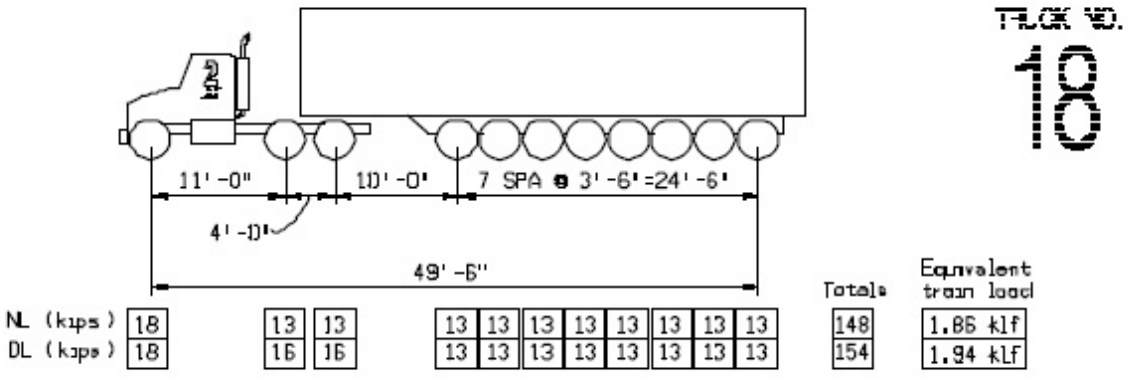

Figure 9
MI-18 truck

Stress contour plots for the plates subjected to the 74.56 kip load can be seen in Figures 10-13; only one end of the plate is shown in Figures 10-13 because of symmetry.

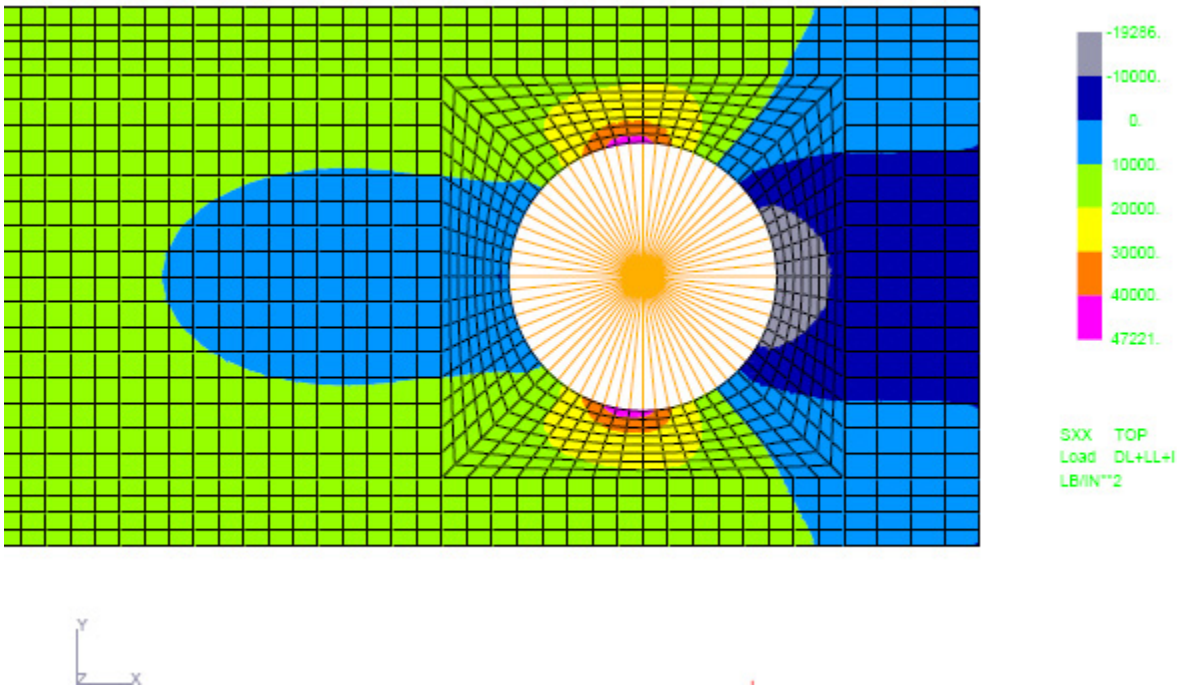

Figure 10
Long plate (AASHTO) S_{xx} stress contour plot (psi)

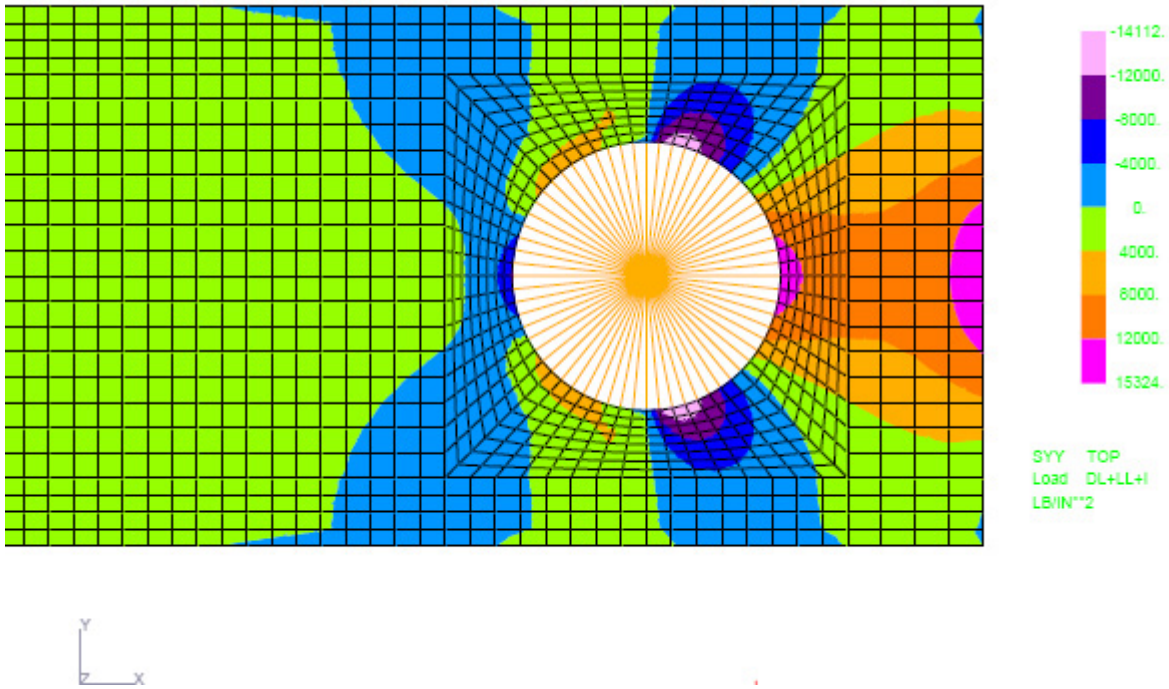

Figure 11
Long plate (AASHTO) S_{yy} stress contour plot (psi)

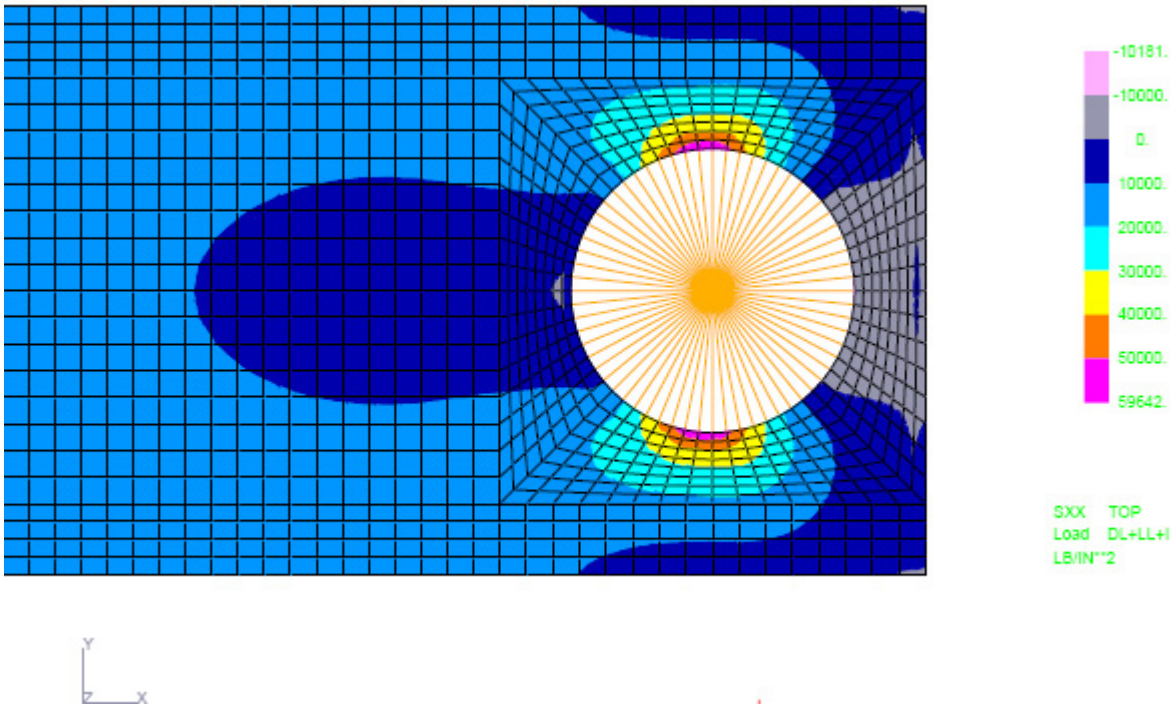

Figure 12
Short plate S_{xx} stress contour plot (psi)

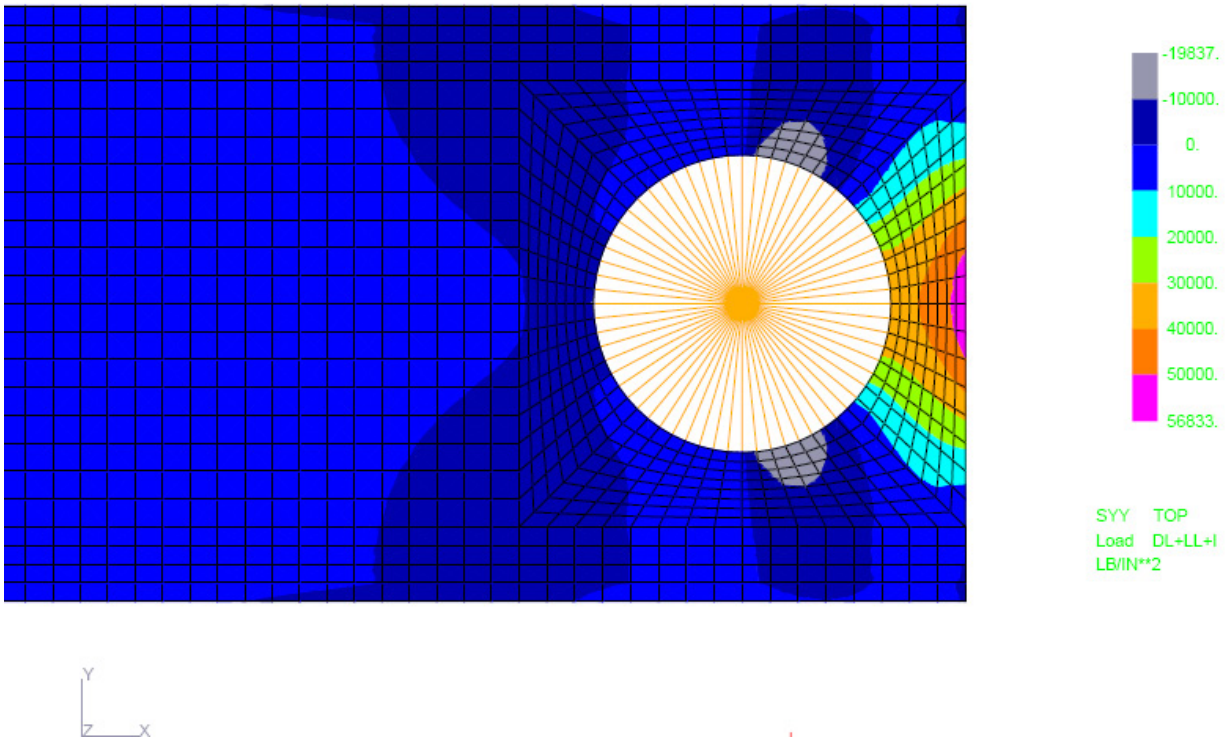

Figure 13
Short plate S_{yy} stress contour plot (psi)

Under the factored load the maximum stresses in the x direction (parallel to the longitudinal axis of the plates), S_{xx}, were 47.2 and 59.6 ksi, for the long and short plates respectively, as seen in Figures 10 and 12. In both cases maximum S_{xx} stresses were located immediately adjacent to the pin-holes, approximately 90 degrees perpendicular to the direction of loading. Maximum stresses in the y direction (perpendicular to the longitudinal axis of the plates), S_{yy}, were 15.3 and 56.8 ksi, for the long and short plates respectively, as seen in Figures 11 and 13. In both cases the maximum S_{yy} stresses were located at the very end of the plates. Bearing stresses (S_{xx}) in the plates from the applied load, located immediately adjacent to the pin-holes were -19.6 and -10.2 ksi, for the long and short plates respectively. Table 1 summarizes the changes in stress from the long to the short link plate.

Table 1
Stress differences at 74.6 kip load
[Tension (+), Compression (-)]

	S_{xx} maximum (ksi)	S_{yy} maximum (ksi)	S_{xx} middle (ksi)	S_{xx} bearing (ksi)
Long Plate	47.2	15.3	10.4	-19.6
Short Plate	59.6	56.8	10.3	-10.2
Stress Increase (%)	26	271	-1	-48

As seen in Table 1, with less material behind the pin, the bearing stress lowers due to reduced stiffness, the stress in the x direction immediately adjacent to the pin-holes increases significantly, and the stress in the y direction at the end of the plate increases dramatically. Although less material significantly affects the stress state around the pin-holes, a considerable portion of the area between the pin-holes is relatively unaffected, as seen in the 'S_{xx} middle' column of Table 1, which represent the stress at the exact middle of the plates. Beginning approximately one pin diameter from the edge of the hole, the stress in the x direction varies between eight and ten ksi for both plates.

4. Specimen Fabrication and Testing

Two link plates were fabricated and tested to verify the FEA. The short plate had the same dimensions as the short plate FEM; the long plate had the same dimensions as the long plate FEM though three inches of material were left behind pin-holes at the non-instrumented end to prevent premature failure at that location. Tensile testing of the link plates was conducted using the 200 kip servo-hydraulic MTS Teststar IIs in MDOT Construction and Technology Division's structural laboratory. The data acquisition system consisted of an Iotech Wavebook with a WBK16 signal conditioning module, using DASYLab V.8 software. Five strain gauges were glued on each link plate at locations of interest based on the modeling. The steel mill certifications listed a yield strength of 46.3 ksi and a tensile strength of 70.8 ksi for the link plate material. Gauge locations and numbers for the link plates can be seen in Figures 14 and 15.

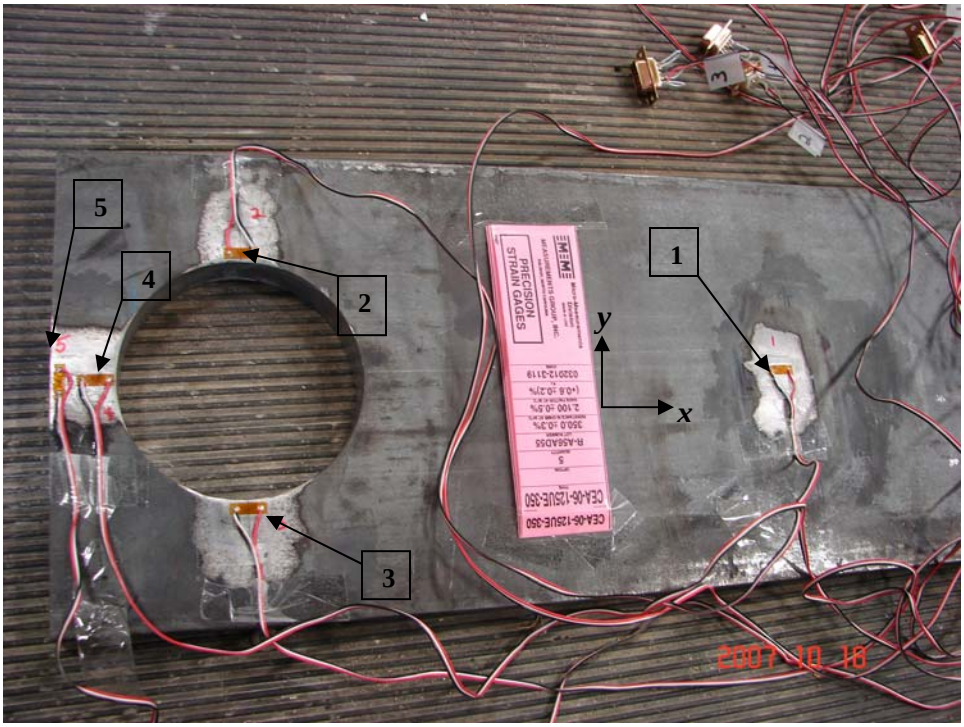

Figure 14
R02-39022 model link plate with strain gauges numbered

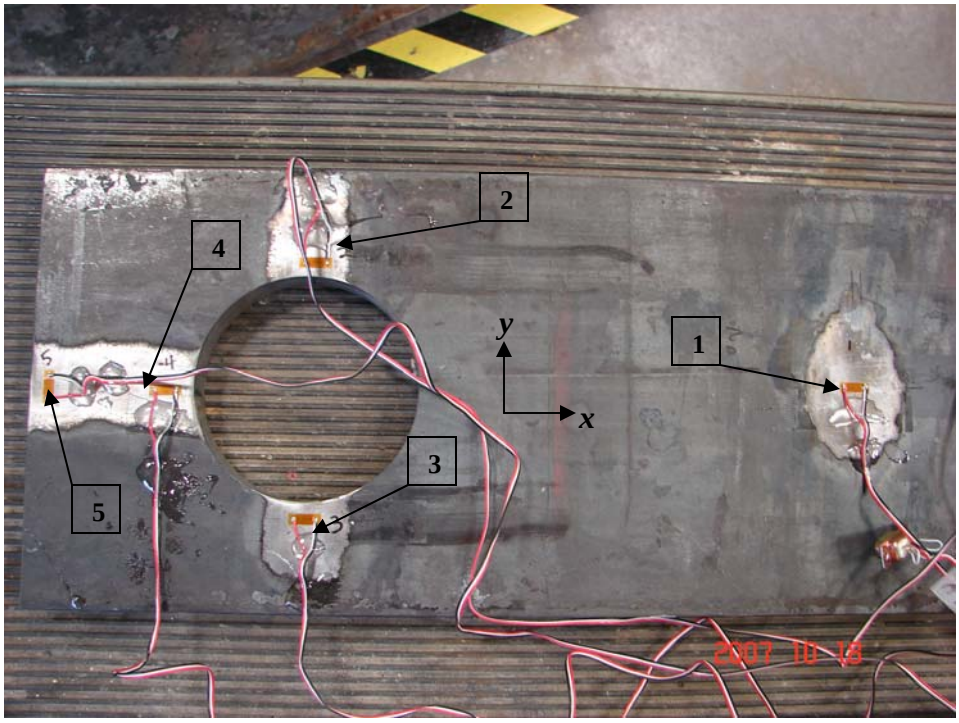

Figure 15
AASHTO model link plate with strain gauges numbered

Both plates were tested using a four inch diameter pin at a loading rate of 10 ksi per minute based on calculations using the area of the net section. Reviewing the testing of the shorter plate (Figure 14), yielding of the steel (based on the mill certification yield strength of 46.3 ksi) was first detected at gauge 5, in the y direction at the end of the link plate, under a load of 53.4 kips. At this load, stresses in the x direction on either side of the hole, at gauges 2 and 3, were 39.4 and 44.6 ksi, respectively. Bearing stress in the x direction at the edge of the hole, at gauge 4, was -3.9 ksi, and the stress at mid plate in the x direction, at gauge 1 was 4.9 ksi. Figure 16 shows the stresses during the test; the horizontally lined portions of the data indicate that the steel had reached the yield plateau. The test was terminated at a load of 108 kips, though gauges 2 through 5 became unglued due to high values of strain before the end of the test.

During the testing of the long plate (Figure 15), yielding was first detected at gauge 3 under a load of 95.8 kips. At this load, stresses at gauges 1, 2, 4, and 5 were 12.5, 37.8, -21.4, and 27.7 ksi, respectively. Figure 17 shows the stresses during the testing of the long plate, which was terminated at a load of 177 kips. Strain gauges 2, 3, and 5 became unglued prior to the conclusion of testing.

The experimental testing provided trends similar to the FEA, the stresses on the side of the pin-holes and at the end of the plate increased significantly from the long plate to the short plate, the bearing stress behind the pin-hole decreased from the long plate to the short plate, and the stresses in the middle of the plates were similar for both tests. However, the experimental stress values did not match the FEA results after yielding because the FEM were linear elastic. The stresses in excess of the yield strength shown previously in Table 1 are not entirely accurate for this reason. As seen in Figures 16 and 17, once the steel reaches its yield strength, the stress

remains constant for some time before increasing once again, which is explained in more detail in section five of this report. The strain gauges became unglued before this secondary increase in stress occurred for the most part, but can be seen in Figure 16 as the slight increase in stress at gauges 2 and 3 immediately before the gauges became unglued. The stresses in Figures 16 and 17 were plotted using the steel properties described in section five of this report.

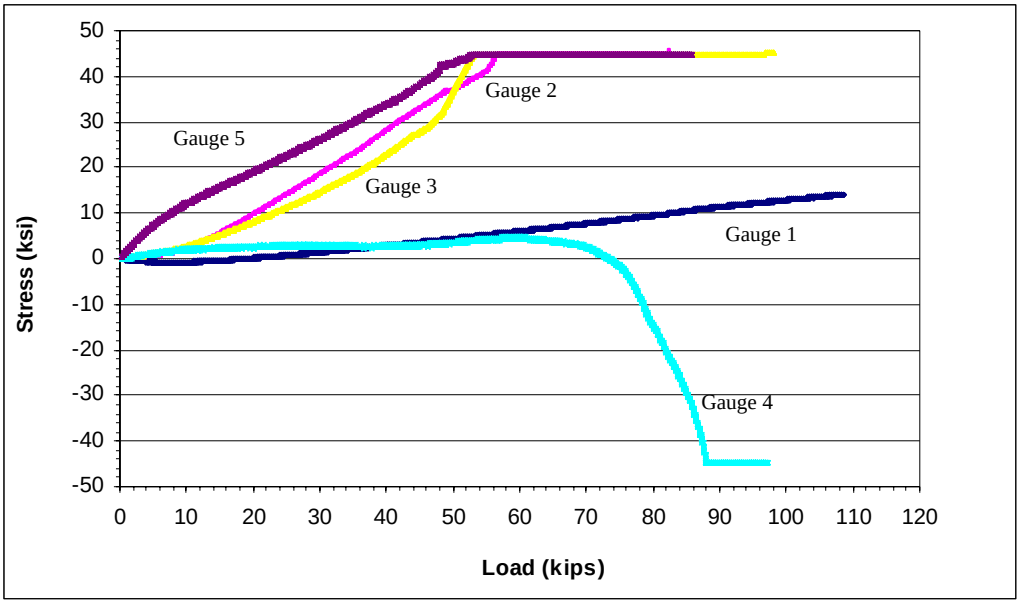

Figure 16
Stress during test of short plate

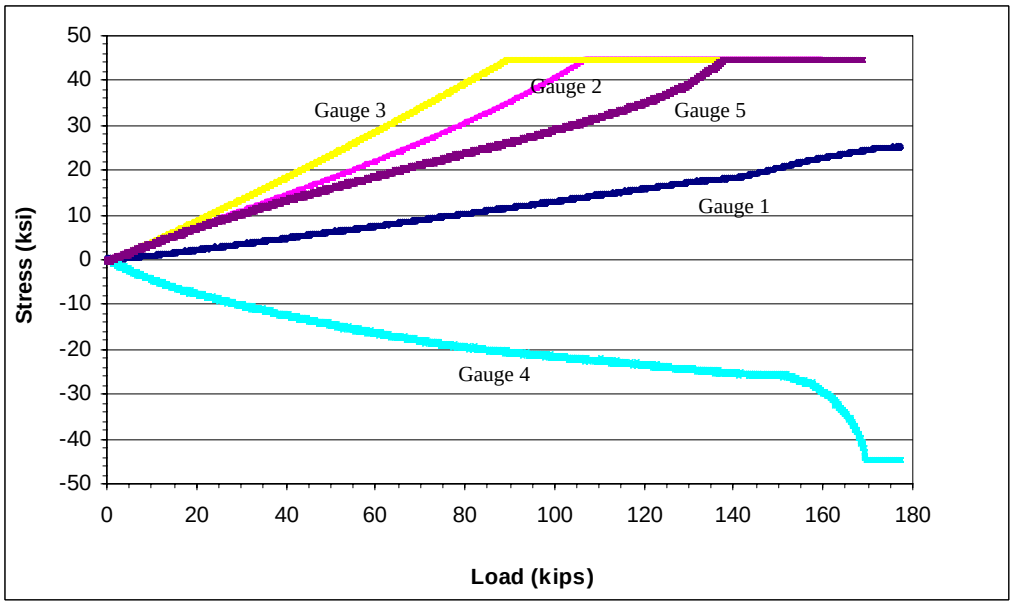

Figure 17
Stress during test of long plate

Figures 18 and 19 show the link plates after tensile testing, which exhibit mill scale loss in the high strain regions adjacent to the pin-hole. Mill scale loss on the long plate was most evident on either side of pin-hole, compared to the short plate where it was more pronounced between the pin-hole and the end of the plate. The mill scale loss corresponds to the high stress regions depicted in the FEM seen in Figures 10-13. No dishing was evident in either of the link plates.

Figure 18
Post-test mill scale loss, link plate with three inches of material behind pin

Figure 19
Post-test mill scale loss, link plate with one inch of material behind pin

5. Nonlinear Finite Element Analysis

To better understand link plate stress distribution, nonlinear FEA was conducted using properties of the steel utilized for experimental testing. Since GTStrudl does not currently support nonlinear elements, elements around the pin-hole were converted to members with the same areas and stiffness, and plastic hinges were placed at the beginning and end of each member. The elements converted to members around the pin-hole can be seen in Figure 20. Each plastic hinge was constructed using a three by seven nodal grid and 12 corresponding fibers, with the in-plate bending defined by two layers of six fibers, as seen in Figure 21. When loaded in bending, the outer fibers will yield first, resulting in a hinge formation, with a linear strain distribution across the section.

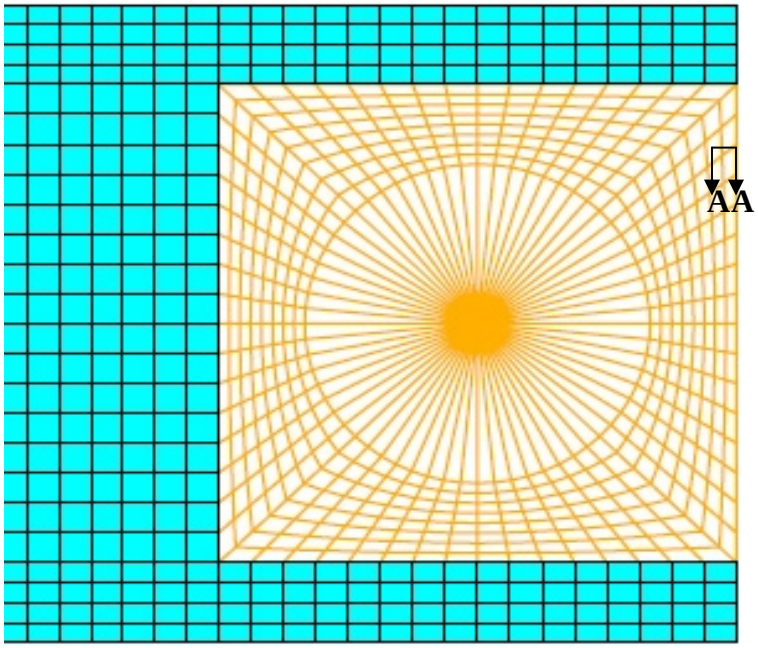

Figure 20
End of nonlinear link plate FEM with one inch of material behind pin, elements around pin converted to members with plastic hinges

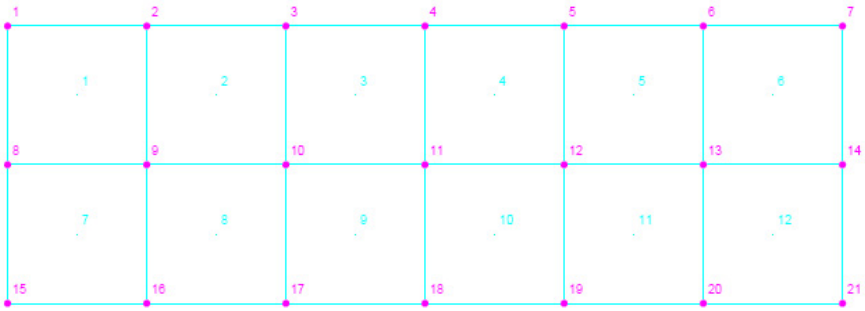

Figure 21
Section A-A,
12-fiber plastic hinge cross-section at beginning and end of nonlinear members

The plastic hinge properties were defined based on testing several samples taken from the middle of the experimental link plates, where the steel had not yielded. These samples were tensile tested with an extensometer and the stress-strain properties derived from testing are shown in Figure 22 and defined in the FEA. [10]

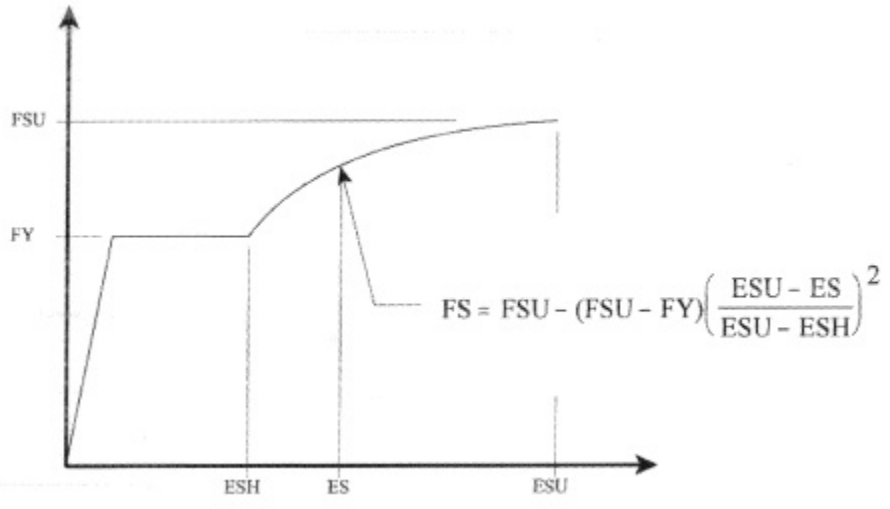

Figure 22
Steel stress-strain curve for plastic hinges in GTStrudl

From the tensile testing of the steel samples, the yield strength determined by the 0.2 percent offset method was 44.6 ksi (FY), the tensile strength was 73.5 ksi (FSU), the yield strain was 0.00154 inch/inch, and the strain at the onset of strain hardening was 0.01246 inch/inch (ESH). The strain at ultimate load was estimated at 0.2154 inch/inch (ESU) by measurement of the tensile testing machine cross-head movement with calipers, as the extensometer was limited to a strain of 0.02125 inch/inch.

As seen in Figures 23 and 24, both the linear and nonlinear models predict the experimental stresses fairly well at the gauge locations when subjected to the factored load of 74.56 kips. It should be noted that the gauge locations, seen in Figures 14 and 15, were slightly offset from the local maximum stress locations – at the very edge of the pin-hole (gauges 2 and 3), and at the end of the plate (gauge 5), noted in Table 1. Also plotted in Figures 23 and 24 is the stress calculated across the net section, $S_{r\ (net\ section)}$, neglecting the stress concentration, as seen in Equation 3, for comparison to experimental and FEA results at gauges 2 and 3.

$$\sigma = \frac{P}{A} = \frac{74.56 kips}{0.875 in \times 4 in} = 21.3 ksi \qquad \text{(Eq.3)}$$

[10] GTStrudl User Reference Manual, Volume 3, "Finite Element Analysis, Nonlinear Analysis, Dynamic Analysis", 2006.

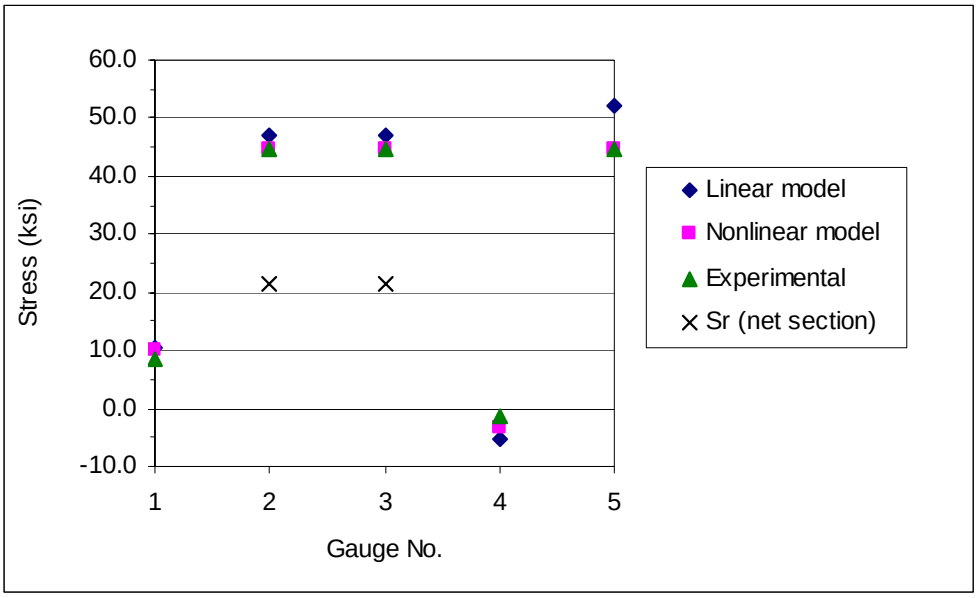

Figure 23
Short plate stress comparison

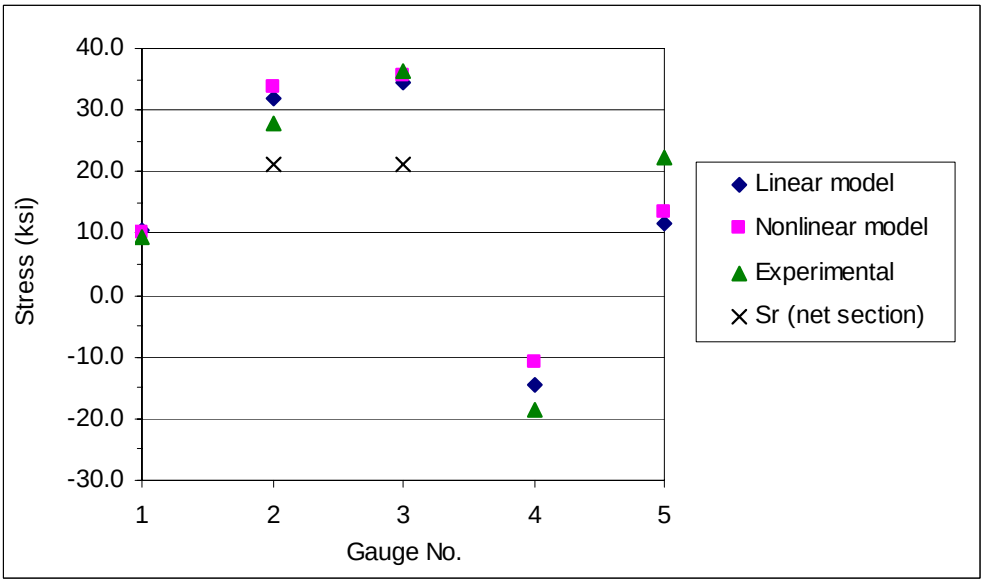

Figure 24
Long plate stress comparison

Both linear and nonlinear FEM of the short plate and long plate were subjected to loads from 30 kips to 180 kips. Figures 25 and 26 illustrate the comparison of the linear and nonlinear FEM to the experimental testing for gauges 2 and 3 on the sides of the pin-holes. For both plates the nonlinear FEM verify the experimental stresses well, before and after yielding, whereas the linear FEA compares well only until yielding occurs.

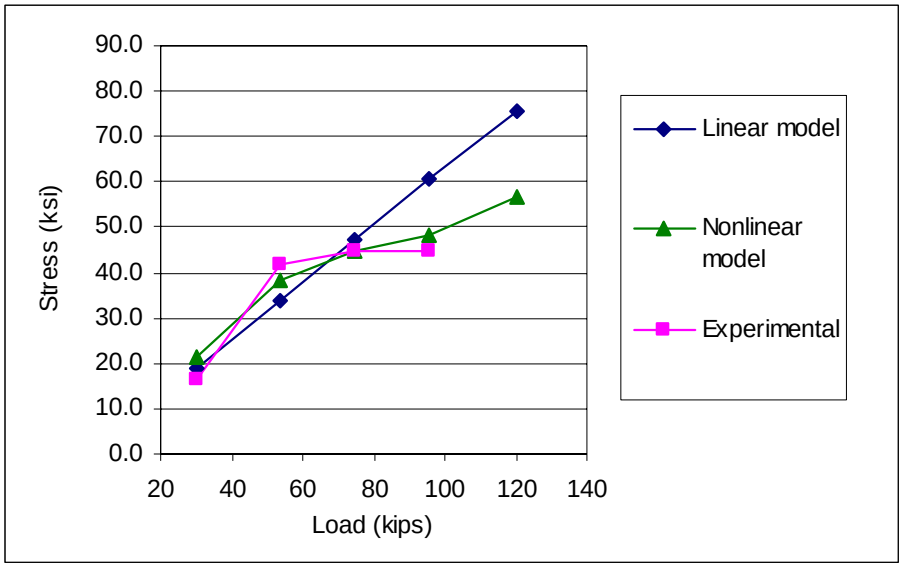

Figure 25
Average of gauge 2 and 3 stresses for short plate

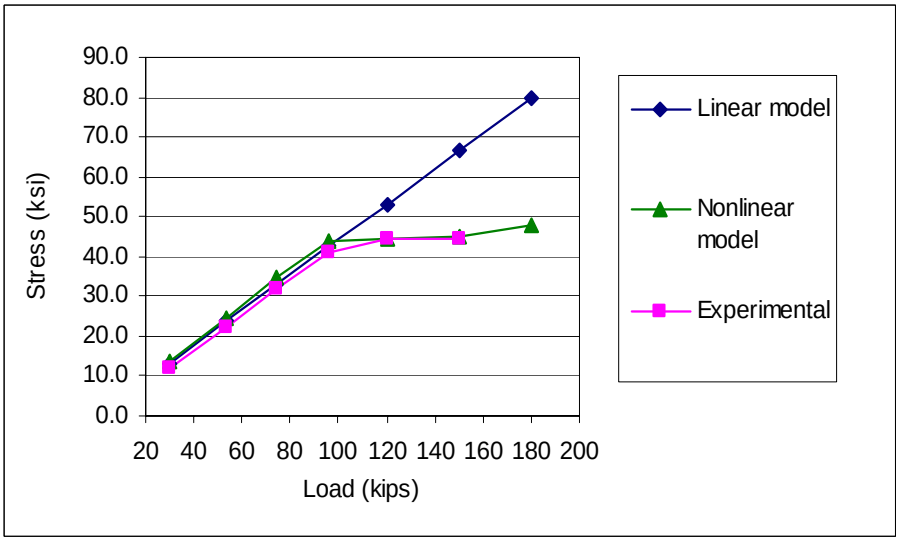

Figure 26
Average of gauge 2 and 3 stresses for long plate

The maximum stresses on the side of the pin-holes were noted in the nonlinear FEA and compared to the stress across the net section neglecting the stress concentrations. Since the actual strain gauges were not at the very edge of the pin-holes, these stresses were slightly higher than the stresses seen in Figures 25 and 26. The calculated stress concentration factors at the edge of the pin-holes were 2.10 for both the long plate and the short plate under the factored loading. These stress concentration factors are consistent with Juntunen's findings. Under unfactored loading neither plate has yielded and the stress concentration of the short plate is 2.60 and the stress concentration of the long plate is 2.09

6. Discussion of Results and Analysis

As seen in Figures 25 and 26, once the side-of-pin steel yields and the load increases, the stress remains at the yield stress for some time before increasing. This can be explained by several factors. Figure 22 shows the stress-strain trace used for modeling the steel properties in the nonlinear FEA, and Figure 27 shows the actual stress-strain trace for the steel used in the experimental testing. In Figure 27, the vertical portion of the trace indicates that the extensometer reached its limit and ceased to record data.

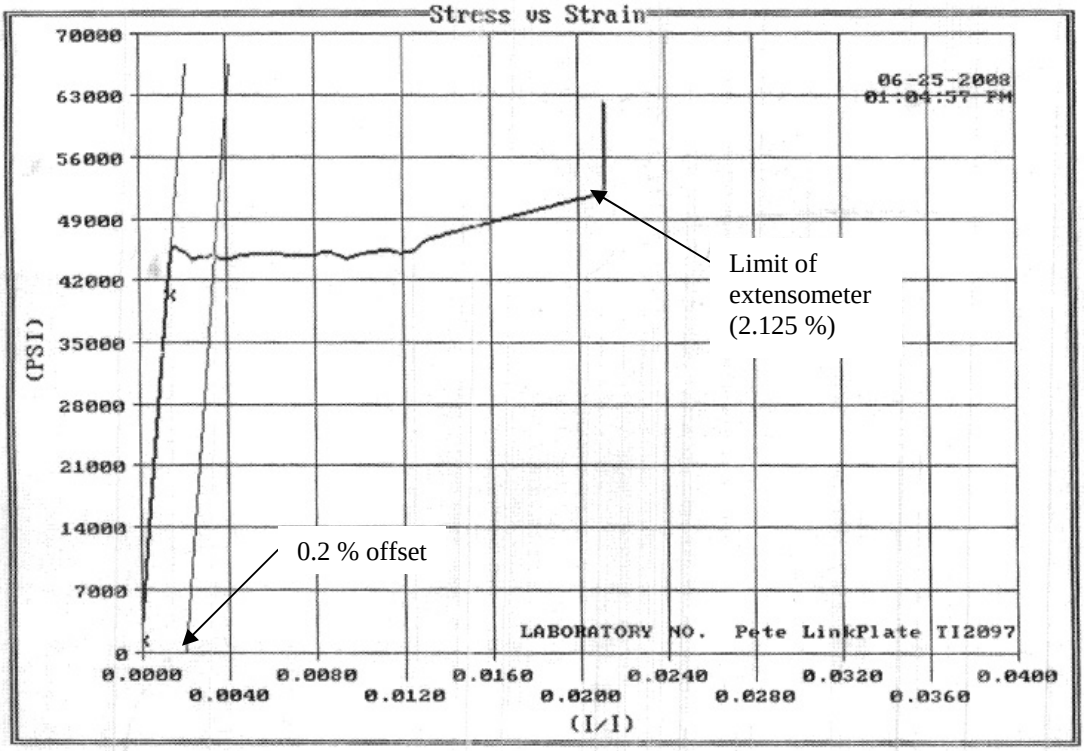

Figure 27
Stress-strain trace for experimental steel link plate tensile sample

The yield plateau shows that there is a relatively large increase in strain, from approximately 0.15 percent to 1.25 percent strain (based on Figure 27), after yielding, before the stress begins increase again. This plateau can also be seen in the results from the experimental testing shown in Figures 16 and 17. This yield plateau also explains why the stress concentration factors were the same for both plates under the factored load of 74.56 kips. Although the stresses were the same, the strains were higher for the short plate and for a given load increase past the yield plateau the stress in the short plate would be higher, due to earlier onset of strain hardening.

The other factor that explains the stress plateau in the link plates is the distribution of stresses across the net section under increased loading. The link plates first yield on the sides of the pin-holes, as seen by the stress concentrations in Figures 10 and 12. It was theorized that as the steel immediately adjacent to the pin-hole strained past yield, additional load was distributed to material further from the pin while the material immediately adjacent to the pin remained at the yield stress. This process was thought to continue until the entire cross section had yielded. At

this point it was believed that the material immediately adjacent to the pin began to strain harden, using a similar process where load is transferred from the inside out across the net section. Tensile failure was thought to occur when the entire cross-section had entered strain hardening, and the material immediately adjacent to the pin reached the breaking strength of the material, fracturing the material from the pin-hole outward to the edge of the plate. Figure 28 illustrates the distribution of load across the net section. Using the nonlinear FEA, the stress and strain were noted immediately adjacent to the pin, one quarter of the distance from the pin to the edge of the plate, and one half of the distance from the pin to the edge of the plate, under varying loads. The plot also shows the stress and strain at the onset of yielding for reference.

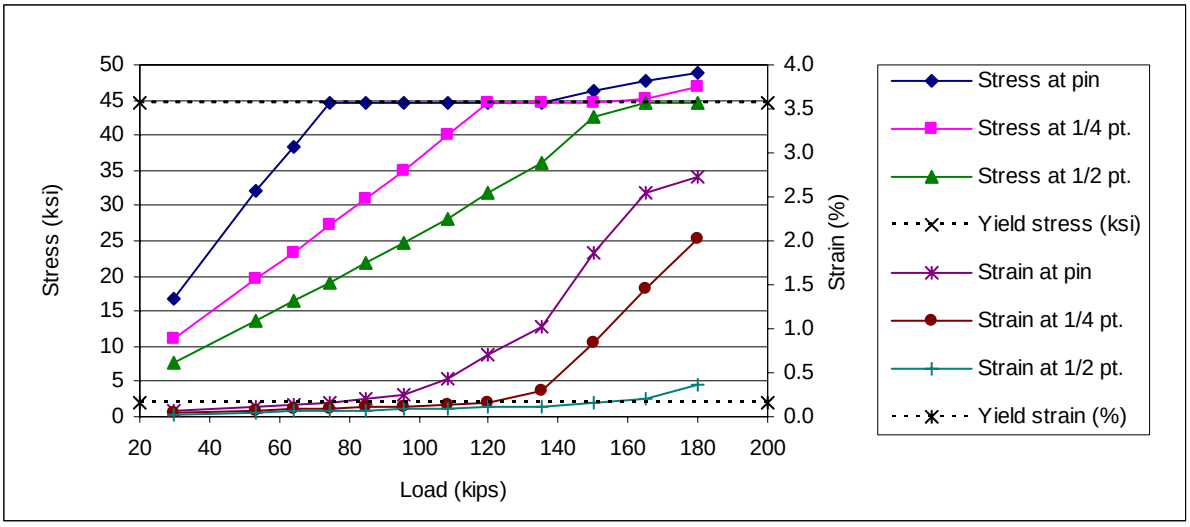

Figure 28
Cross-section stress and strain distribution of the long plate (nonlinear FEA)

As seen in Figure 28, the side of the pin-hole yields first, at which point it remains at the yield stress, and while it continues to strain, stress increases further out from the pin-hole. Shortly after the stress at the one quarter point reaches the yield stress, the stress at the pin-hole begins to strain harden and experiences an increase in stress. When the stress at the one half point reaches the yield stress, the stress at the one quarter point begins to strain harden and experiences an increase in stress. Similar results were obtained with the shorter plate, as seen in Figure 29.

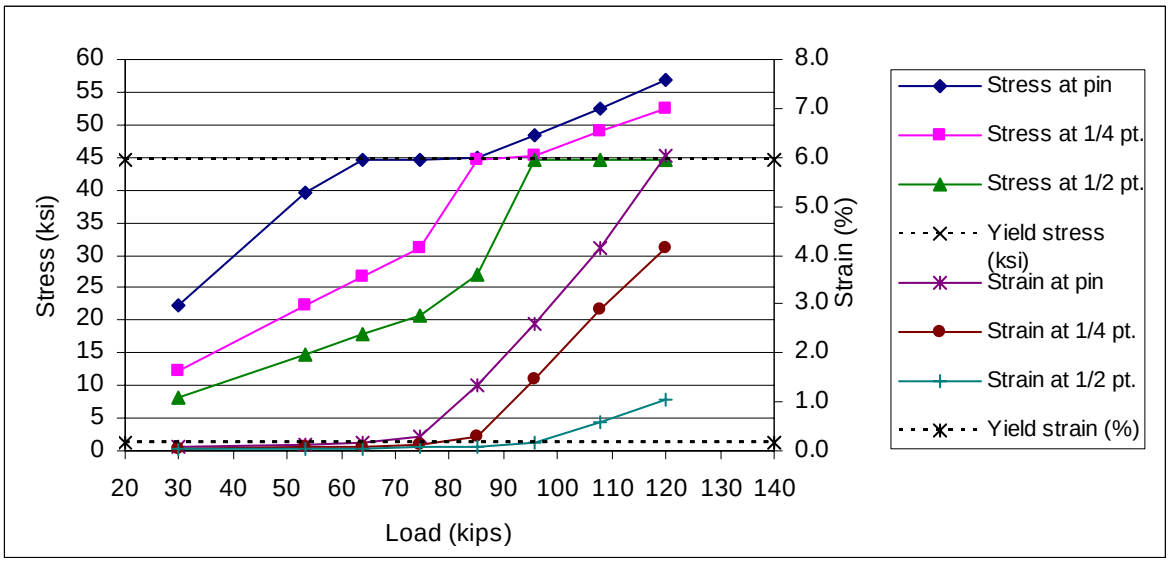

Figure 29
Cross-section stress and strain distribution of the short plate (nonlinear FEA)

With the nonlinear data verified by the experimental data and the distribution of load, stress, and strain investigated for a given link plate, additional FEM were created to study the effect of varying amounts of material behind the pin in link plates. The FEM were created with 1.5 inches and 2.0 inches of material behind the pin, in addition to the original models with 1.0 inches and 3.0 inches of material behind the pin. A model with the minimum required length material behind the pin, 2.4 inches, was also created, and the models were subjected to an unfactored service load of 42.0 kips. The service load was chosen to allow a comparison between the different FEM before yielding occurred.

Figure 30 illustrates the effect on stresses as the amount of material behind the pin is varied from the minimum design value, when the service load of 42.0 kips is applied. The point of intersection of the curves in Figure 30 represents a link plate with the minimum required area behind the pin. Stresses on either side of the pin-hole (S_{xx}) and at the end of the plate (S_{yy}) increase nonlinearly as material behind the pin is reduced, with the trend more pronounced for the stresses at the end of the plate. Bearing stress (S_{xx}) decreases nonlinearly as material is removed from behind the pin and the mid plate stress (S_{xx}) remains relatively unchanged, decreasing less than one percent as the material behind the pin is changed from three inches to one inch.

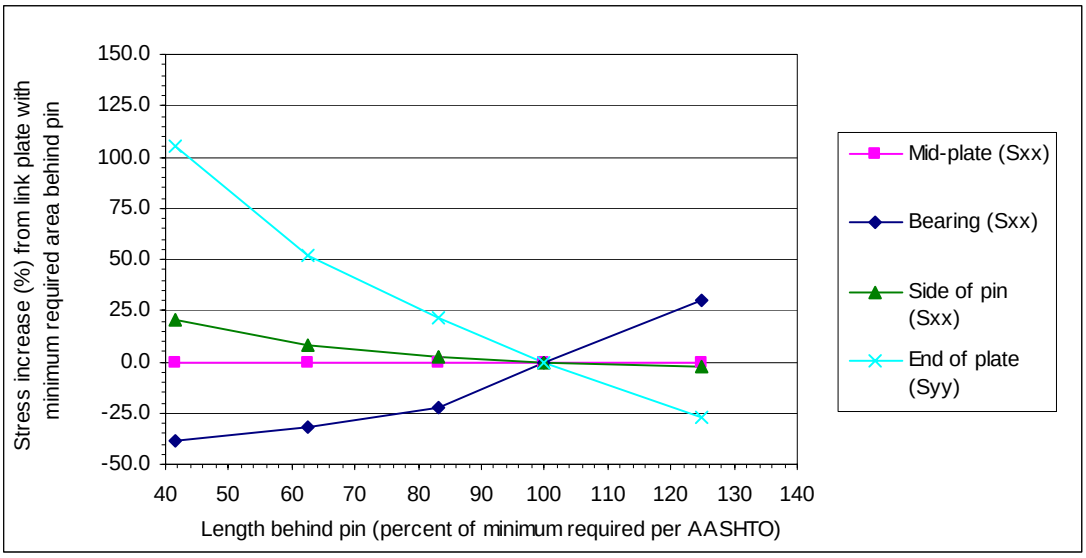

Figure 30
Stresses for link plates with varying amounts of material behind the pin compared to the minimum required area behind pin (nonlinear FEA), 42.0 kip service load applied

Based on the nonlinear FEA, Figure 31 was created to show the stress concentration factors for the maximum stresses in x direction immediately adjacent to the pin (S_{xx}), and at the end of a link plate (S_{yy}), as a function of the length of material behind the pin. The y-axis represents the ratio of maximum stresses from the nonlinear FEA to the stress calculated across the net section not accounting for stress concentrations. The x-axis represents the ratio of the length of material behind the pin to the minimum length of material behind the pin specified by AASHTO. The unfactored service load of 42.0 kips was used to develop Figure 31 in order to show the variation between link plates with varying lengths of material behind the pin. If the factored loading had been used, a significant number of the link plate models would have yielded and shown similar or equal stress concentration factors due to their stress state presence along the yield plateau. As seen in Figure 31, when the length of material behind the pin-hole is greater than specified by AASHTO, the effect on the side-of-pin stress is minor, and the stress concentration factors are consistent with the experimental testing and Juntunen's findings. When the length of material behind the pin-hole is less than specified by AASHTO, the side-of-pin stress concentration factor increases nonlinearly, as do the end-of-plate stress concentration factors, though more dramatically. In Figure 31, the side-of-pin stress concentration factor at 208 percent of the minimum length required is 2.04, and appears to approach a value of 2.00 as the length behind the pin goes to infinity, similar to the stress concentration factor of 2.15 calculated using Equation 2.

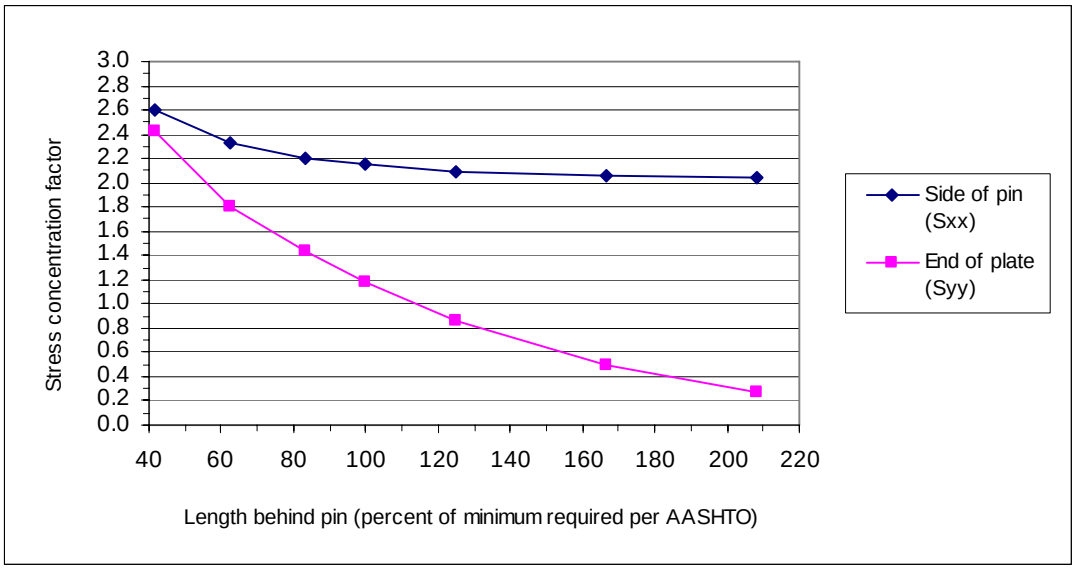

Figure 31
Stress concentration factors for link plate stresses adjacent to the pin and at the end of the link plate (nonlinear FEA)

In order to develop a method for estimating effective stresses in link plates when the material behind the pin is less than required by AASHTO, two approaches were investigated. First, curve-fitting equations for stress concentration were developed for the data in Figure 31. Second degree rational polynomials were found to provide the most efficient curve-fitting equations; the least squares solution for third degree rational polynomials provided a negligible increase in accuracy. Normalizing the equations to the stress concentration in the link plate with the minimum required length of material behind the pin per AASHTO, the equation for the maximum side-of-pin stress concentration factor, is

$$\phi_{Sxx} = 0.8826 + 10.2838R^{-1} + 138.2543R^{-2} \qquad \text{(Eq.4)}$$

and the equation for the maximum end-of-plate stress concentration is

$$\phi_{Syy} = -0.3351 + 154.6686R^{-1} - 2313.2030R^{-2} \qquad \text{(Eq.5)}$$

where:

ϕ_{Sxx} = side-of-pin stress concentration factor, normalized to AASHTO requirement
ϕ_{Syy} = end-of-plate stress concentration factor, normalized to AASHTO requirement
R = length behind pin as a percent of the minimum required length behind pin per AASHTO

To compensate for additional stress concentrations in non-standard link plates, Equation 4 and Equation 5 can be applied to the basic calculation of the stress across the net section in link plates neglecting the stress concentration factors. The estimated effective side-of-pin stress is

$$\sigma_{Sxx} = \phi_{Sxx} \frac{P}{2A_n} \quad \text{(Eq.6)}$$

and the estimated effective end-of-plate stress is

$$\sigma_{Syy} = \phi_{Syy} \frac{P}{2A_n} \quad \text{(Eq.7)}$$

where:

σ_{Sxx} = stress in the link plate adjacent to the pin in the direction of loading (ksi)
σ_{Syy} = stress at the end of the link plate perpendicular to the direction of loading (ksi)
P = factored load applied to the entire link plate assembly (kips)
A_n = area of the net section through the pin-hole of one link plate (in^2)

Because stress concentrations exist in correctly fabricated link plates, which can cause localized yielding, Equations 4 and 5 were normalized to the correctly designed link plate to allow a useful comparison. To estimate the actual localized maximum stresses in a link plate, the stress concentration factors, ϕ_{Sxx} and ϕ_{Syy}, could be taken from Figure 31 and not Equations 4 and 5. With stress concentration factors from Figure 31, resulting stresses in excess of the material yield strength would indicate that the material has yielded, but may be on the yield plateau and not stressed to the level calculated.

The second approach applied was developed by Johnston[11]. Since localized yielding occurs in link plates long before yielding of the entire cross-section and subsequent failure, a "general yield point" of the plate was defined as the load at which the slope of the curve of load plotted against deformation between pin and plate (about three pin diameters away) is three times the initial slope. For the link plates used in this project, the deformation used represents the difference between the longitudinal deformations of the pin and the center of the plate. Using nonlinear FEA for link plates with varying lengths of material behind the pin subjected to varying loads, the loads were plotted against the deformations as seen in Figure 32.

[11] *Pin-connected Plate Links*, American Society of Civil Engineers, Johnston, Bruce G., 1939.

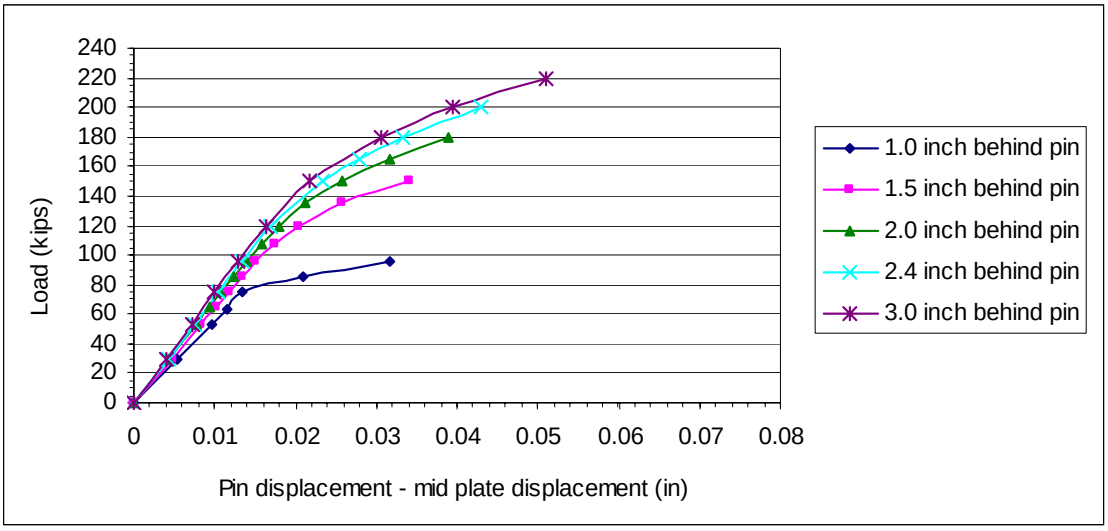

Figure 32
Load versus displacement (nonlinear FEA)

As expected, as the length of material behind the pin is increased, the displacement for a given load decreases. The "general yield point" is more obvious and occurs earlier, with respect to both load and displacement, as the length of material behind the pin is decreased. Figure 33 shows the calculated loads at which the slopes of the curves are three times the initial slopes. The calculated loads were normalized to the general yield load of the link plate with the minimum required material behind the pin.

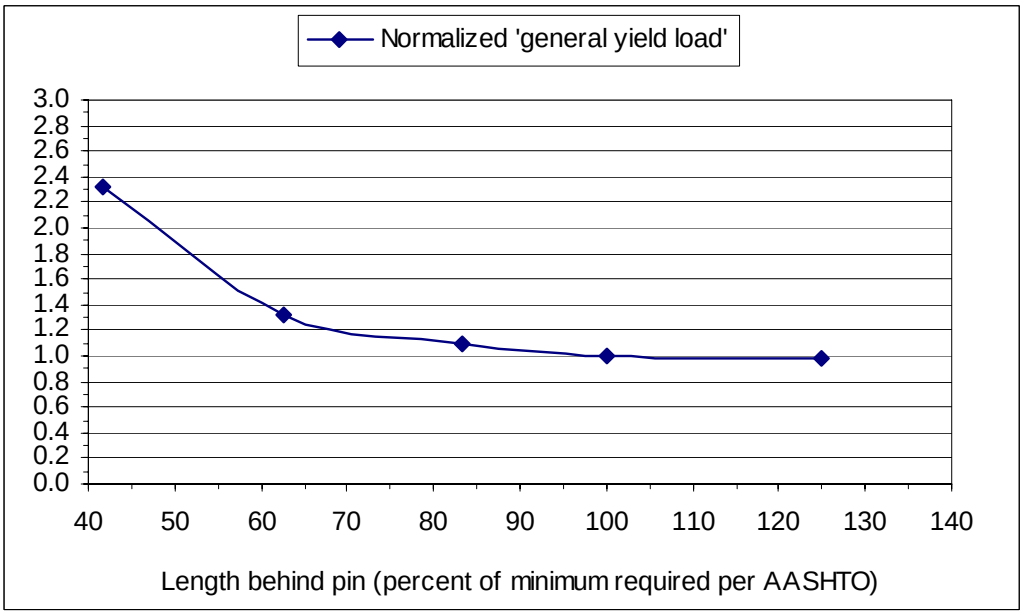

Figure 33
"General yield loads" for link plates with varying length of material behind pin, normalized to yield load with the minimum required material behind the pin

Developing an equation to fit the data in Figure 33,

$$\phi_g = 1.2579 - 73.7781R^{-1} + 4913.3525R^{-2} \qquad \text{(Eq.8)}$$

where:

ϕ_g = "general yielding" load factor
R = length behind pin as a percent of the minimum required length behind pin per AASHTO

The estimated effective "general yielding" stress is

$$\sigma_g = \phi_g \frac{P}{2A_n} \qquad \text{(Eq.9)}$$

where:

σ_g = effective "general yielding" stress of the link plate (ksi)
P = factored load applied to the entire link plate assembly (kips)
A_n = area of the net section through the body of one link plate (in^2)

The "general yield" approach takes into account the performance of the plate as a whole, whereas the stress concentration approach provides a means of calculating localized maximum stresses. As seen in Figure 34, the effective stress factors determined using the two methods provide somewhat similar results.

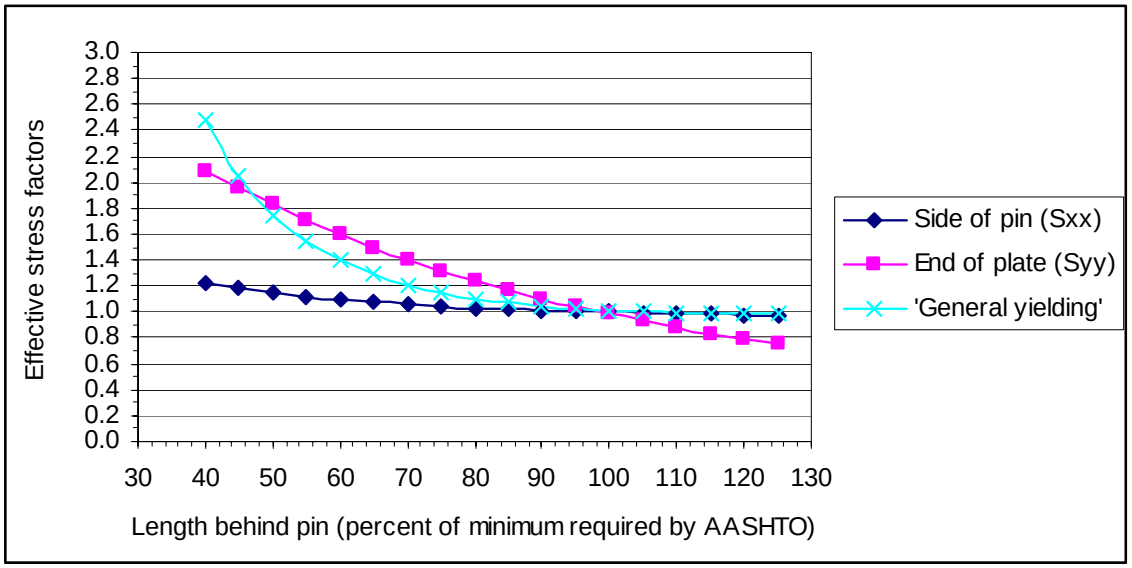

Figure 34
Stress concentration method and general yielding method of determining effective link plate stresses for varying lengths of material behind link plate pins

Using Equations 6 and 7, the effective stresses in the R02-39022 link plate with one inch of material behind the pin under the factored load of 74.56 kips, would be 25.8 ksi for side-of-pin and 43.6 ksi for end-of-plate, compared to the calculation of stress across the net section neglecting any stress concentration of 21.3 ksi under the same load. These stresses account for the stress concentrations that are developed in a correctly fabricated plate. Therefore, under the factored load, the R02-39022 link plate shows a small to moderate increase in stress adjacent to the pin-hole and a large increase in stress at the end of the plate. If the actual localized maximum stresses are calculated substituting in the stress concentration factors from Figure 29, the side-of-pin and end-of-plate stresses for the link plate with one inch of material behind the pin are 55.4 ksi and 51.7 ksi, respectively, indicating both areas have yielded. For the link plate with the minimum allowable length of material behind the pin, the side-of-pin and end-of-plate local maximum stresses would be 45.8 ksi and 25.1 ksi, respectively, indicating the material adjacent to the pin has yielded, but the material at the end of the plate has not.

Using Equation 9, the effective "general yield" stress for the short plate is 49.4 ksi, indicating yielding. For the link plate with the minimum allowable length of material behind the pin, the effective "general yield" stress is 21.5 ksi, similar to the net section stress not accounting for stress concentrations of 21.3 ksi. Although the side-of-pin material has yielded, however, the overall performance of the plate can be considered acceptable.

It should be noted that Equations 4 through 9 were developed based on link plates with eight inch widths and four inch diameter pins, a ratio of plate width to pin radius of four to one. Other link plate geometries used by the department[12,13] are listed in Table 3; along with the respective stress concentrations calculated using Equation 2. The increase in stress concentration from the plate width to pin-hole radius ratio equal to 4.0, which was used in development of Equations 4 through 9, is also shown.

As seen in Table 2, the D/r ratio is proportional to the stress concentration, though the variation between different link plate and pin combinations used by MDOT is relatively small. Therefore, to estimate the effective stress when using Equations 6, 7, and 9 for link plates with a D/r ratio greater than 4.0, the stress can be increased by a percentage similar to the last column of Table 3.

[12] MDOT Bridge Design Guides 8.14.01-8.14.02, *Pin Design Table*, 1985, 1980, 1976, 1971, 1966.
[13] MDOT Research Report R-1358, *Study of Michigan's Link Plate Assemblies*, 1998.

Table 2
Department link plate geometries and stress concentrations

Pin-hole radius, r (in)	Plate width, D (in)	D/r ratio	Stress concentration factor, k (from Equation 2)	Increase from D/r = 4.0 (percent)
1.5	7	4.67	2.21	2.28
1.5	8	5.33	2.26	4.49
2	8	4.00	2.16	0.00
2	8.5	4.25	2.18	0.86
2	9	4.50	2.20	1.71
2.25	9	4.00	2.16	0.00
2.5	9	3.60	2.13	-1.35
2.75	10	3.64	2.13	-1.23
3	15	5.00	2.24	3.40

7. R02-39022 Material Properties

Samples were taken from one of the salvaged link plates from R02-39022 to compare the steel material properties in different portions of the link plate and to verify the stress distribution evident from the nonlinear FEA. Two of the samples were taken on either side of the pin-hole and one sample was taken from the middle of the plate. The samples taken from the side-of-pin area were located as close as possible to the edge of the pin-hole; however, because of the material needed for gripping the samples during tensile testing, the center of the gauge length of the samples was offset approximately one inch from the center of the pin-hole along the longitudinal axis of the link plate. The side-of-pin samples were taken immediately adjacent to the pin-hole, as seen in Figure 35. The mid-plate sample was taken several inches away from the true middle of the plate, though previous FEA modeling showed the stress anywhere between the pin-holes to be relatively low.

Figure 35
Salvaged link plate from R02-39022, samples tested for material properties

Table 3 shows the yield strength, tensile strength, elongation, and reduction of area for the three tensile samples taken from the link plate shown in Figure 35.

Table 3
Material properties of R02-39022 link plates

Sample location	Yield Strength (ksi)	Tensile Strength (ksi)	Elongation (percent)	Reduction of Area (percent)
Mid-plate	34.2	66.1	42.9	64.1
Side of pin - A	45.2	70.3	32.4	64.2
Side of pin - B	44.8	68.0	27.3	64.8
Side of pin - Avg.	45.0	69.2	29.9	64.5

As seen in Table 3, the steel adjacent to the pin has a 32 percent higher yield stress, a 4.7 percent higher tensile stress, and a 30.3 percent lower elongation from the sample in the middle of the plate. This indicates that the steel adjacent to the pin had previously been loaded past yield. In determining the yield strength of the samples, an extensometer was used to plot the stress-strain trace, and for the mid-plate sample the 0.2% offset method was used. When examining the stress-strain traces of the side-of-pin samples it was evident that previous loading had caused strain hardening to begin. Therefore, upon tensile testing there was no yield plateau and the new yield point was clearly defined. From the tensile testing data it is evident that the material adjacent to the pin-hole had reached a stress of at least 45.0 ksi, and adjacent to the center of the pin-hole the stress reached was estimated at 48.2 ksi based on the nonlinear FEA results. This is verified by the fracture locations on the tensile specimens adjacent to the pin-hole in Figure 35, which are to the left of the center of the samples. Since the material closest to the center of the pin-hole would have yielded first and reached a higher stress, material further away would have a lower yield point and be the point of weakness in the tensile samples.

There was not enough remaining material adjacent to the pin-hole of the salvaged R02-39022 link plates available for evaluating the effect of yielding on fracture toughness. Reviewing previous research[14,15] indicated that steel damaged beyond yield and then heat straightened can have reduced fracture toughness. However, in these cases the damage strains were beyond what the R02-39022 link plates experienced, and fracture toughness testing was conducted after heat straightening. Testing conducted by MDOT[16] on A-36 steel stressed beyond the original yield strength of 45 ksi, to 52 ksi, found that the mean fracture toughness decreased 46 percent. An unpaired *t*-test indicated that the probability of the null hypothesis, that the unyielded and yielded data were statistically similar, was between 0.01 and 0.001.

[14] MDOT Research Report RC-1476, *Effects of Multiple Damage-Heat Straightening Repair on the Fundamental Properties of Bridge Steels*, 2004.
[15] NCHRP Report 604, *Heat Straightening Repair of Damaged Steel Bridge Girders: Fatigue and Fracture Performance*, 2008.
[16] *Effect of Yielding on Fracture Toughness of A-36 Steel*, Jansson, Peter O., 2008.

8. Conclusions and Recommendations

FEA was performed to investigate the stress distribution and determine the effects on performance of link plates with less than the required amount of material behind the pin as specified by AASHTO. Experimental testing verified the nonlinear FEA and it was discovered that reducing the amount of material behind the pin causes moderate stress increases adjacent to the pin and large stress increases at the end of a link plate, while bearing stress on the link plate and stress in the middle of a link plate remain relatively unaffected. The overall performance of a link plate with reduced material behind the pin was also shown to have been decreased substantially.

Equations were developed to estimate the actual side-of-pin and end-of-plate local maximum stresses based on the length of material behind the pin, and normalized to the stress concentrations that would be expected in a link plate designed with the proper amount of material behind the pin. Since local maximum side-of-pin stresses are at least twice that of side-of-pin stresses neglecting stress concentrations, even in link plates with the required amount of material behind the pin, local yielding can occur under factored loading. However, as demonstrated in the experimental testing and nonlinear FEA, under loading twice that which caused the initial localized yielding, only small deformations were evident in the properly designed link plate. Initial yielding is restrained from rapid progress by the surrounding low stressed areas. Therefore, in evaluating the overall capacity or performance of a link plate, "general yielding" should be considered. The R02-39022 link plate experienced general yielding at 43 percent of the load that caused general yielding of the link plate with the minimum length of required material behind the pin. It is believed that the ultimate capacity would be similarly affected.

A salvaged link plate from R02-39022 was shown to have yielded and begun strain hardening in the area adjacent to the pin-hole. As a result, the localized material properties were changed as follows: yield strength increased, tensile strength increased, ductility decreased, and fracture toughness decreased. When comparing the R02-39022 link plate to a link plate with the AASHTO specified amount of material behind the pin, the general yield strength and ultimate capacity are decreased, and the fatigue resistance is decreased because of the higher stress range.

Although this investigation concentrated on the effects of the length of material behind the pin, it is expected that there would be a correlation to link plates with the proper length of material behind the pin but reduced thickness due to corrosion. Although reduced thickness can cause "dishing" failure, lateral restraint provided to link plates by the pin-nut and beam would likely prevent this.

The following recommendations are made.

1. Link plates with a "general yield" stress, as determined by Equation 9, in excess of the material yield strength should be removed and replaced.

2. Link plates with less than the required amount of material behind the pin that have localized stresses as determined by Equations 6 and 7 in excess of the material yield strength, should be removed and replaced.

3. Investigate the effect on stress distribution and capacity of link plates due to corrosion induced section loss.

9. References

AASHTO (2002). *Standard Specifications for Highway Bridges*, 16th Edition, Washington D.C.

AASHTO (2007). *LRFD Bridge Design Specifications*, Fourth Edition, Washington D.C.

American Railway Engineering Association (1911). *Manual of the American Railway Engineering Association: Definitions, Specifications, and Principles of Practice*, Chicago, IL.

American Railway Engineering Association (1921). *Manual of the American Railway Engineering Association: Definitions, Specifications, and Principles of Practice*, Chicago, IL.

ASTM International (2007). ASTM A370-01, *Standard Test Methods and Definitions for Mechanical Testing of Steel Products,* West Conshohocken, PA, 2007.

Connor, R. J. et al (2008). *Heat Straightening Repair of Damaged Steel Girders: Fatigue and Fracture Performance,* NCHRP Report 604, Washington D.C.

Georgia Institute of Technology (2007). GTStrudl User Reference Manual, Volume 3, *Finite Element Analysis, Nonlinear Analysis, Dynamic Analysis*, Revision T, Atlanta, GA.

Jansson, Peter O. (2008). MDOT Memorandum, *Effect of Yielding on Fracture Toughness of A-36 Steel*, Lansing, MI.

Jansson, Peter O. (2008). Personal communications with MDOT personnel from Design Division and Construction and Technology Division, Lansing, MI.

Johnston, Bruce G. (1939). *Pin-Connected Plate Links,* American Society of Civil Engineers, Journal of the Structural Division, Reston, VA.

Juntunen, D. A. (1998). MDOT Research Report R-1358, *Study of Michigan's Link Plate Assemblies*, Michigan Department of Transportation, Lansing, MI.

Michigan Department of Transportation (2003). *MDOT Bridge Analysis Guide*, Lansing, MI.

Michigan Department of Transportation (1985, 1980, 1976, 1971, 1966). MDOT Bridge Design Guides 8.14.01-8.14.02, *Pin Design Table*, Lansing, MI.

Varma, Amit H., Kowalkowski, Kieth, J. (2004). *Effects of Multiple Damage-Heat Straightening Repair on the Fundamental Properties of Bridge Steels*, Michigan Department of Transportation, Lansing, MI.

Young, Warren, C. (1989). *Roark's Formulas for Stress and Strain*, Sixth Edition, McGraw-Hill, Inc.